Final Technical Report

Regional Scale Dynamical Modelling of Biogeochemical Processes

AD-A240 115

Allan R. Robinson
Principal Investigator
Gordon McKay Professor of Geophysical Fluid Dynamics
Division of Applied Sciences
Harvard University

91-08102

This project involved the design and development of 3D regional biogeochemical models. The biogeochemical models were designed for attachment to the Harvard Hierachy of models, including the surface boundary layer (SBL) component (Walstad and Robinson, submitted, 1991) of the open ocean baroclinic eddy resolving quasigeostrophic (QG) model (Miller, Robinson and Haidvogel, J. of Comp. Physics, **50**:38–70,1981), or its coastal extensions (Milliff, Math. and Comp. in Simul., **31**:541–564,1989; and Ozsoy,Lozano and Robinson, Ibidem, In Press,1991) (SBL/QG), and the open boundary primitive equation (PE) model with hybrid vertical coordinates (Spall and Robinson, Math. and Comp. in Simul., **31**:241–269, 1989). The selection of these physical models is motivated by the interest to study the time evolution of biogeochemical components with realistic physical fields, as they all have data assimilation schemes associated.

The approach taken in biogeochemical model design was to construct first simplified models with a minimal number of biogeochemical components, and then step-by-step to introduce further components and detailed intercomponent interactions. These simplifications allow focused research on important biological mechanisms in the presence of realistic

DISCLAIMER NOTICE
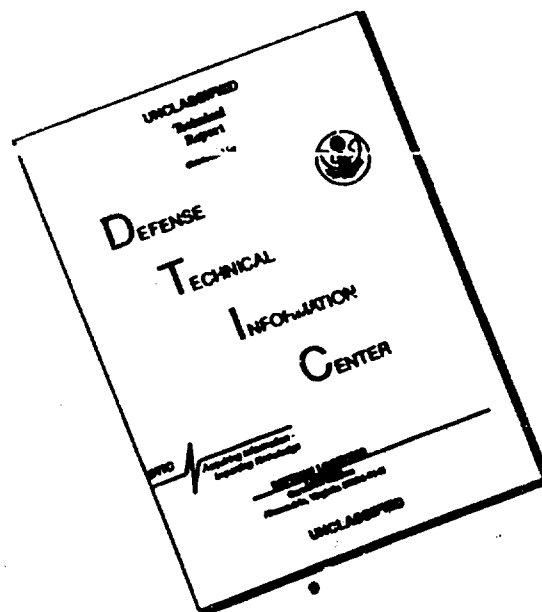
THIS DOCUMENT IS BEST QUALITY AVAILABLE. THE COPY FURNISHED TO DTIC CONTAINED A SIGNIFICANT NUMBER OF PAGES WHICH DO NOT REPRODUCE LEGIBLY.

physical fields. The construction of regional biogeochemical models with data assimilation schemes will provide a unique tool to determine processes and sensitivities operative in the real ocean and to facilitate efficient experimental design and model validation.

The lead scientists at Harvard in the first stage were Dr. Fred Lipschultz and Dr. Carlos J. Lozano. This initial effort was interrupted when Dr. Lipschultz took a position at the Bermuda Biological Station. In the second stage, Dr. Mark Altabet (WHOI) undertook the responsibilities of Dr. Lipschultz until the termination of this contract. In the following paragraphs we outline the main results achieved within the contract period.

The simplest biogeochemical model of interest is of the nitrogen cycle. During this contract we constructed two models with two different compartmentalizations of the nitrogen components. The simplest physical model resolving realistically physical fields of importance to biogeochemical processes is the SBL/QG model. However, in the model implementation a modular approach has been taken in order to facilitate the insertion of biogeochemical models in either the QG or PE models and thus to allow the biogeochemical models to be driven by fields produced by either model. In the QG configuration extensive sensitivity studies can be carried out for given sets of 4D physical fields. The PE configuration is used for benchmarking physical processes. Within the biogeochemical models similarly a modular approach has been taken to allow the exploration of different compartmentalizations, cycles (e.g., C) and interaction parameterization.

During the first stage of this project Dr. Lipschultz designed and implemented a 3D biogeochemical model with three nitrogen compartments, namely phytoplankton nitrogen, zooplankton nitrogen and dissolved inorganic nitrogen that includes both nitrate and ammonium (PZD model). Growth of phytoplankton is either light or nutrient limited using equations from Kiefer and Mitchell (Limnol. Oceanogr., 28: 770-776,1983). Zooplankton grazing are described by equations from Franks et al (Mar. Biol., 91: 121-129,1986). The

nutrient field below the mixed layer is initialized by the relationship with salinity based on Elrod and Kester (Deep Sea Res., **33**:1313–1325,1986).

At the time of his departure to Bermuda, Dr. Lipschultz has completed the coding for a 3D version of the model attached to the SBL/QG model, and the initial stages of calibration were underway. Upon arrival to the Biological Station in Bermuda he ported the codes to a minicomputer. Dr. Lipschultz continues to maintain a close scientific relationship with members of the group; and his modular 3D implementation facilitates the construction of the 3D version of the biogeochemical model designed and tested during the second stage of the project.

Dr. Altabet's experience with nitrogen cycles and his direct access to data and its interpretation led to the development of a second version biogeochemical model in terms of three nitrogen compartments, namely small nitrogen particulates, big nitrogen particulates and dissolved inorganic nitrogen (SBD model). In this model big nitrogen particulates sink due to gravity providing a nitrogen recirculation path towards the lower portions of the water column. Dr. Carlos Lozano designed, implemented and carried out the numerical calibration of a one-dimensional version of the model as a first step to the 3D model. The essential requirements imposed to the numerical algorithm were the 'mass' conservation, the maintenance of nonnegative values for of each nitrogen compartment and an efficient treatment of the fast time scale related to big particulates sinking rates. Subsequently, Dr. Altabet carried out extensive biogeochemical calibration and sensitivity studies of the SBD model in a parameter range appropriate for the Bermuda area. Both the seasonal and interannual cycles show good qualitative agreement with observed data, and the model response to parameter changes is adequate. This work will be used to calibrate the 3D version of the model. Further details are contained in the appended internal report which is an integral part of this final report.

Even though no immediate publications have been produced during the contract period, substantial progress was made in model design and development and the investigators have accomplished the fundamental basis for a significant interdisciplinary modelling effort based on realistic physical fields.

A 1-dimensional Upper Ocean Biogeochemical Model:
Calibration and Simulations for the Bermuda Area

M. Altabet[1] and C. J. Lozano[2]

August 6, 1990

1. Introduction

In this report we describe the formulation, numerical implementation, and calibration of a 1-dimensional biogeochemical (BGC) model to be attached to the Harvard Open Ocean Surface Boundary Layer Model (Lozano, Walstad and Robinson, 1990). The BGC model has been constructed with the following attributes:

1) The BGC model is capable of simulating near-surface nitrate fluxes, new production, and particle flux with a relatively small number of compartments and interactions (Figure 1). A basic premise for our effort is that a principal influence of ocean physics on biology and chemistry is through the transport of nitrate into the euphotic zone. This flux combined with nitrogen export from the euphotic zone in the form of large, fast-sinking particles determines population sizes and particle concentrations. Hence instead of a classical NPZ formulation (nitrate, phytoplankton, zooplankton) we have chosen a 3-compartment, NSB formulation (nitrate[DIN], small particles [SPN], large particles [BPN]) to reflect the importance of the export term. These modeled quantities can be easily compared to field data such as those found in Altabet (1989, Limnol. Oceanogr.). Phytoplankton are an implicit component of the SPN. Euphotic zone recycling of nitrogen which is a function of zooplankton and bacterial activity is also not explicit in this first version of the model since it does directly influence new production.

---

[1] Woods Hole Oceanographic Institute

[2] Harvard University

2) The model is capable of high vertical resolution in the upper 200 m. In oligotrophic oceans, high-light, low nutrient strata overlay low-light, high nutrient strata giving rise to vertical structure in particle concentration and fluxes. In 3-D simulators, nutrient fluxes are likely to be sensitive to both the vertical gradients in light and phytoplankton and along isopycnal gradients in nitrate. As discussed in the results section, simulation of vertical structure is an important test of model validity. High vertical resolution will also be important for comparison of simulated chlorophyll concentration with remotely sensed data (and conversely its assimilation into the model) since strong subsurface chlorophyll maxima are persistent features of the open ocean. The biogeochemical model (Fasham et al., submitted to *J. Mar. Res.*) which has been attached to the Princeton U. 3-D physical model (basin scale coarse grid) only considers the mixed layer without any vertical structure.

The uptake of nitrate (DIN) into small particles (SPN) is the principal non-linear term of the model and is dependent upon nitrate concentration, small particle concentration, and light intensity. The dependencies on light and nitrate concentration are hyperbolic. Light levels decrease exponentially with depth as a function of the extinction coefficient which in future versions will be derived from SPN concentrations. The fraction of SPN which is active phytoplankton and the fraction of total N uptake which is the form of nitrate are presently fixed parameters but also will be variable in future versions with more complex trophic structure. Interconversion between small and large (BPN) particles are simple first-order processes with fixed parameters. The breakup of large particles is thought to be as significant as their formation in the ocean. Downward particle flux is the product of BPN concentration and sinking speed (fixed parameter). SPN decay and production of nitrate is considered as single, first ordered process inhibited by light since nitrification is known to be strongly inhibited within the euphotic zone.

In the 1-D model physical parameters are defined externally. We have included (Figure 1b) short wave radiation I, vertical diffusivity discontinuous at the base of the mixing layer.

2

A mixed layer of specific depth and K_z can be specified. Below the mixed layer, K_z is set to lower specified value and vertical advection. These parameters can be time varying in order to simulate daily, seasonal, or yearly cycles.

Section 2 states the model governing equations and some of its integral properties are presented in Section 3. The numerical solution algorithms are contained in Section 4; diagnosis variables are introduced in Section 5. Boundary conditions for the runs described in Section 6 are: 1) no flux at surface and 2) no flux at bottom boundary. The model is, however, presently capable of having fluxes through the bottom based on gradients in its vicinity. Our final conclusions are drawn in Section 7.

2. Governing Equations

In the first-order model P_0 we consider an ocean with no mean motions and the significant spatial variations occur in the vertical only. The ambient effects are the vertical light distribution, the varying time and space diffusivities — mostly due to variation in mixing layer depth, the biogeochemical fluxes at the bottom, and vertical advection due to fluid motions.

We now establish some notation and state an initial boundary-valued problem. Let

$$n(z,t) = [n^{(1)}, n^{(2)}, n^{(3)}] = [\text{SPN}, \text{BPN}, \text{DIN}], \tag{1}$$

denote the state vector dependent upon vertical position z and time t. Here z is positive upwards with the origin at the water surface.

The time evolution of the state variables is given by

$$L[n] = \partial_t n - M[n]n - \frac{\partial}{\partial z}\left(K\frac{\partial n}{\partial z}\right) + W\frac{\partial n}{\partial z} = 0, \tag{2}$$

$$(z,t) \in D \quad \text{with} \quad D = \{(z,t) \mid t \geq 0, \ -h \leq z \leq 0\},$$

where the species local interactions is described by the first term on the right-hand side with

$$M[u] = \begin{bmatrix} \lambda(z,t)\frac{f_p n^{(3)}/t_{max}}{n^{(3)}+\bar{n}^{(3)}} - k_{12} - k_D(z,t) & k_{21} & 0 \\ k_{12} & -k_{21} & 0 \\ -\lambda(z,t)\frac{f_p n^{(1)}/t_{max}}{n^{(3)}+\bar{n}^{(3)}} + k_D(z,t) & 0 & 0 \end{bmatrix}, \tag{2a}$$

The functions λ and k_D depend upon incoming short wave radiation and here are given by

$$\lambda(z,t) = \frac{I_z}{I_z + \hat{I}_z}, \tag{2b}$$

4

$$k_D(z,t) = k_{D\max} \left(1 - \frac{I_z}{I_z + \hat{I}_D} \right) , \tag{2c}$$

with

$$I_z = I_0(t) \exp[z/z_0] , \tag{2d}$$

The exchange coefficients k_{12}, k_{21} are constant. The diffusivity tensor is taken to be diagonal

$$K = \begin{bmatrix} K^{(1)} & 0 & 0 \\ 0 & K^{(2)} & 0 \\ 0 & 0 & K^{(3)} \end{bmatrix} , \tag{2e}$$

and only the second component, BPN, sinks, i.e., the advection matrix W is given by

$$\mathbf{W} = \begin{bmatrix} w & 0 & 0 \\ 0 & w - w_{\text{sink}} & 0 \\ 0 & 0 & w \end{bmatrix} ; \qquad w_{\text{sink}} \geq 0 , \tag{2f}$$

and w is the fluid vertical velocity.

In the sequel we will consider the initial boundary-valued problem (2) with initial conditions

$$\mathbf{n}(z,0) = \hat{\mathbf{n}}(z) ; \quad \hat{n}^{(j)}(z) \geq 0 , \quad j = 1, 2, 3 , \tag{3}$$

and boundary conditions

$$\mathbf{B}_0[\mathbf{n}] = \mathbf{K} \frac{\partial \mathbf{n}}{\partial z} - \mathbf{W}\mathbf{n} \bigg|_{z=0} = 0 , \tag{4}$$

$$\mathbf{B}_h[\mathbf{n}] = \mathbf{K} \frac{\partial \mathbf{n}}{\partial z} - \mathbf{W}\mathbf{n} \bigg|_{z=-h} = -\mathbf{f}(t) \qquad \mathbf{f} = [f^{(1)}, f^{(2)}, f^{(3)}] , \tag{5}$$

i.e., at the free surface there are no fluxes and at the bottom of the biologically active water column there are fluxes. Normally we will assume an influx of dissolved nitrogen

$$f^{(3)}(t) \geq 0 , \tag{6a}$$

5

into the domain; no flux of small particulates

$$f^{(1)}(t) = 0 , \tag{6b}$$

and big particulates do not enter the system

$$f^{(2)}(t) \leq 0 . \tag{6c}$$

The main objective of this note is the numerical solution of the initial boundary-valued problem (2), (3)-(5) referred to as problem P_0.

We introduce the shorthand writing $n > 0$ for $n^{(j)} > 0$; $j = 1, 2, 3$. A function $V(z,t)$ is an upper solution to P_0 in D if

$$L[V] \geq 0 ; \qquad (z,t) \in D , \tag{7a}$$

$$V(z,0) \geq n(z) ; \qquad -h \leq z \leq 0 , \qquad \cdot \tag{7b}$$

$$B_0[V] > 0 ; \qquad 0 \leq t \leq t_{max} , \tag{7c}$$

$$B_h[V] > f ; \qquad 0 \leq t \leq t_{max} . \tag{7d}$$

A lower solution v satisfies (7) with the inequalities reversed.

We are interested only on nonnegative solutions ($n \geq 0$) of P_0. This problem, we shall prove later on, has upper and lower solutions; but in general the least upper solution V^* and the largest lower solution v^* may not coincide; that is $v^* \leq V^*$ with the strict inequality holding in some portion of Domain D. To ascertain uniqueness or multiplicity of solutions and the concomitant solution bifurcations it is necessary to establish a more restrictive set of assumptions on P_0. In Section 4 a numerical algorithm is proposed assuming a unique solution.

3. Nitrogen Content

In the sequel, the property of the matrix M in (2a)

$$\sum_{i,j=1}^{3} M_{ij} n^{(j)} = 0 \; , \tag{8}$$

is essential. For the sake of clarity, consider first the special case $w^{(1)} = w^{(3)} = 0$, $w^{(2)} = -w_{\text{sink}}$, with w_{sink} depth independent. The nitrogen content defined by

$$N = \sum_{j=1}^{3} n^{(j)} \; , \tag{9a}$$

satisfies the equation

$$\partial_t N = \frac{\partial}{\partial z} \left[\sum_{j=1}^{3} K^{(j)} \frac{\partial n^{(j)}}{\partial z} - w^{(2)} n^{(2)} \right] \; . \tag{9b}$$

In particular if $K^{(1)} = K^{(2)} = K^{(3)} = K$ we can write the last equation in the form

$$\partial_t N = \frac{\partial}{\partial z} \left[K \frac{\partial N}{\partial z} \right] - \frac{\partial}{\partial z} \left(w^{(2)} n^{(2)} \right)$$

i.e., the nitrogen content diffuses in the water column with diffusivity K and has a sink of strength $\frac{\partial}{\partial z} \left(w^{(2)} n^{(2)} \right)$.

Returning to (9) we find that the total nitrogen content in the water column

$$\bar{N}(t) = \int_{-h}^{0} N(z, t) \, dz \; , \tag{10a}$$

satisfies the relation

$$\frac{d\bar{N}}{dt} = \sum_{j=1}^{3} \left[K^{(j)} \frac{\partial n^{(j)}}{\partial z} - w^{(2)} n^{(j)} \delta_{j2} \right] \Bigg|_{-h}^{0} \; . \tag{10b}$$

7

The time evolution of the total nitrogen content satisfies the ordinary differential equation

$$\frac{d\bar{N}}{dt} = \sum_{j=1}^{3} f^{(j)}(t) \,, \tag{11a}$$

with initial conditions

$$\bar{N}(0) = \int_{-h}^{0} \left(\sum_{j=1}^{3} \hat{n}^{(j)}(z) \right) dz \,. \tag{11b}$$

In general, $w^{(j)} \neq 0$ and the fluid vertical divergence $\partial w / \partial z = -\text{div} \, u$ is not necessarily zero. Indeed, within the mixing layer

$$\partial w / \partial z \sim \frac{\partial}{\partial x} \left(\frac{\tau_y}{\rho_0 f h_m} \right) - \frac{\partial}{\partial y} \left(\frac{\tau_x}{\rho_0 f h_m} \right) + \frac{\partial w_Q}{\partial z} \,, \tag{12}$$

where $\vec{\tau} = (\tau_x, \tau_y)$ in the wind stress, ρ_0 the density of the water, f the Coriolis parameter, h_m the depth of the mixing layer, and w_Q is the interior vertical velocity. Below the mixing layer only the latter term remains. The total nitrogen content then is given by

$$\frac{d\bar{N}}{dt} - \sum_{j=1}^{3} \int_{-h}^{0} \frac{\partial w^{(j)}}{\partial z} n^{(j)} \, dz = \sum_{j=1}^{3} f^{(j)}(t) \,. \tag{13}$$

We shall use the total nitrogen content time history governed by (13) and (11b) to monitor the quality of the numerical solution.

4. Numerical Model

In our application w_{sink} is two orders of magnitude larger than w; that is, the sinking process of big particulates has a fast time scale $t_S \sim h/w_{\mathrm{sink}}$ relative to diffusivity time scales $t_b \sim h^2/K$ or advection time scales $t_a \sim h/w$. In our first algorithm we do not exploit this time scale differences; whereas in the second algorithm we use a time splitting technique to avoid the refined grids required to resolve adequately the sinking process.

4.1 First algorithm.

(a) Time Step

A completely implicit time step algorithm of (2) yields the two-level scheme

$$\frac{n^{\mathcal{J}+1} - n^{\mathcal{J}}}{\Delta t} - M[n^{\mathcal{J}+1}]n^{\mathcal{J}+1} - \partial_z[K^{\mathcal{J}+1}\partial_z n^{\mathcal{J}+1}] + W\partial_z n^{\mathcal{J}+1} = 0 \qquad \mathcal{J} \geq 1 , \quad (14a)$$

$$n^0 = \hat{n} , \qquad (14b)$$

where $n^{\mathcal{J}} = n(z, \mathcal{J}\Delta t)$, $\mathcal{J} = 0, 1, \ldots$, and Δt is the time step.

The nonlinear equation (14a) is solved iteratively as follows: Given initial data

$$y_0 = n^{\mathcal{J}} , \qquad (15a)$$

and positive numbers $\epsilon^{(j)}$; $j = 1, 2, 3$, compute y_p; $p \geq 1$, such that

$$y_p - \Delta t D^{\mathcal{J}+1}[y_{p-1}]y_p - \Delta t \partial_z[k^{\mathcal{J}+1}\partial_z y_p] + \Delta t W \partial_z y_p = n^{\mathcal{J}} + \Delta t N[y_{p-1}]y_{p-1} ; \qquad p \geq 1$$

$$(15b)$$

9

where

$$D^{J+1} = \begin{bmatrix} m_{11} & 0 & 0 \\ 0 & m_{22} & 0 \\ 0 & 0 & 0 \end{bmatrix} \qquad N^{J+1} = \begin{bmatrix} 0 & m_{12} & 0 \\ m_{21} & 0 & 0 \\ m_{31} & 0 & 0 \end{bmatrix}, \qquad (15c)$$

and boundary conditions

$$B_0[y_p] = 0 \qquad B_h[y_p] = f^{J+1}, \qquad (15d)$$

until

$$|y_p^{(j)} - y_{p-1}^{(j)}| < \epsilon^{(j)}; \qquad j = 1, 2, 3. \qquad (16)$$

Comment. The nonlinearity in (14a) arises from the terms m_{11} and m_{32}; and the splitting of (2a)

$$M = D + N$$

achieves the uncoupling of species in the left-hand side of (14a) allowing fast simple algorithms.

We now focus our attention in the boundary linear differential equation problem (15b)–(15d). After the substitutions $y_p^{(j)} \to y^{(j)}$; $y_{p-1} \to \mathcal{Y}_{\text{prev}}^{(j)}$ we have:

$$y^{(1)}[1 - \Delta t (m_{11}[y_{\text{prev}}^{(3)}])^{J+1}] - \Delta t \partial_z[(K^{(1)})^{J+1}\partial_z y^{(1)}] + \Delta t(w^{(1)})^{J+1}\partial_z y^{(1)} = f_c^{(1)}, \quad (17a)$$

$$y^{(2)}[1 - \Delta t (m_{22})^{J+1}] - \Delta t \partial_z[(K^{(2)})^{J+1}\partial_z y^{(2)}] + \Delta t(w^{(2)})^{J+1}\partial_z y^{(2)} = f_c^{(2)}, \qquad (17b)$$

$$y^{(3)} - \Delta t \partial_z[(K^{(3)})^{J+1}\partial_z y^{(3)} + \Delta t(w^{(3)})^{J+1}\partial_z y^{(3)} = f_c^{(3)}, \qquad (17c)$$

with

$$f_c^{(1)} = (n^{(1)})^J + \Delta t(m_{12})^{J+1}\mathcal{Y}_{\text{prev}}^{(2)}, \qquad (18a)$$

10

$$f_c^{(2)} = (n^{(2)})^{\mathcal{J}} + \Delta t (m_{21})^{\mathcal{J}+1} \mathcal{Y}_{\text{prev}}^{(1)}, \tag{18b}$$

$$f_c^{(3)} = (n^{(3)})^{\mathcal{J}} + \Delta t (m_{31})^{\mathcal{J}+1} \mathcal{Y}_{\text{prev}}^{(1)} + \Delta t (m_{32})^{\mathcal{J}+1}, \tag{18c}$$

and boundary conditions

$$(K^{(1)})^{\mathcal{J}+1} \partial_z (y^{(1)}) - (w^{(1)})^{\mathcal{J}+1} \partial_z y^{(1)} = 0 ; \qquad \text{at} \quad z = 0 \tag{19a}$$

$$(K^{(2)})^{\mathcal{J}+1} \partial_z (y^{(2)}) - (w^{(2)})^{\mathcal{J}+1} \partial_z (y^{(2)}) = 0 ; \qquad \text{at} \quad z = 0 \tag{19b}$$

$$(K^{(3)})^{\mathcal{J}+1} \partial_z (y^{(3)}) - (w^{(3)})^{\mathcal{J}+1} \partial_z y^{(3)} = 0 ; \qquad \text{at} \quad z = 0 \tag{19c}$$

$$(K^{(1)})^{\mathcal{J}+1} \partial_z (y^{(1)}) - (w^{(1)})^{\mathcal{J}+1} \partial_z y^{(1)} = 0 \qquad \text{at} \quad z = -h , \tag{20a}$$

$$(K^{(2)})^{\mathcal{J}+1} \partial_z (y^{(2)}) - (w)^{\mathcal{J}+1} \partial_z (y^{(2)}) = -(f^{(2)})^{\mathcal{J}+1} \qquad \text{at} \quad z = -h , \tag{20b}$$

$$(K^{(3)})^{\mathcal{J}+1} \partial_z (y^{(3)}) - (w^{(3)})^{\mathcal{J}+1} \partial_z y^{(3)} = -(f^{(3)})^{\mathcal{J}+1} . \tag{20c}$$

(b) 1-D Boundary Problem

We use finite differences to solve (17)–(19). Let $zml_\ell = -h < zml_{\ell-1} < \ldots < zml_1 < zml_0 = 0$ be a partition of the interval $-h \leq z \leq 0$ and set

$$dzml_k = -zml_k + zml_{k-1} ; \qquad k = 1, \ldots, \ell .$$

11

Setting $\mathcal{Y}_k = y(zm\ell_k)$ we approximate (17) by

$$\mathcal{Y}_k^{(j)}(1 - \Delta t m_{jj}) - \frac{2\Delta t}{dzm\ell_k + dzm\ell_{k-1}}\left[-\frac{K_k^{(j)}}{dzm\ell_k}(\mathcal{Y}_k^{(j)} - \mathcal{Y}_{k-1}^{(j)}) + \frac{K_{k+1}^{(j)}}{dzm\ell_{k+1}}(\mathcal{Y}_{k+1}^{(j)} - \mathcal{Y}_k^{(j)})\right]$$

$$+ \frac{\Delta t}{dzm\ell_k + dzm\ell_{k-1}}\left[\left(w_{k-1}^{(j)}\mathcal{Y}_{k-1}^{(j)} - w_{k+1}^{(j)}\mathcal{Y}_{k+1}^{(j)}\right) - \mathcal{Y}_k^{(j)}\left(w_{k-1}^{(j)} - w_{k+1}^{(j)}\right)\right]$$

$$= fc_k^{(j)} = n_k^{(j)} + \Delta t \sum_{i=1}^{3} N_{ji}\left[(\mathcal{Y}_k^{(\ell)})_{\text{prev}}\right]\mathcal{Y}_{\text{prev}}^{(i)}; \qquad 1 \le k \le \ell - 1, \quad j = 1,2,3 ,(21)$$

and boundary conditions

$$\frac{K_1^{(j)}}{dzm\ell_1}[\mathcal{Y}_0^{(j)} - \mathcal{Y}_1^{(j)}] - \frac{1}{2}w_0^{(j)}\mathcal{Y}_0^{(j)} - \frac{1}{2}w_1^{(j)}\mathcal{Y}_1^{(j)} = 0; \qquad j = 1,2,3 . \tag{22}$$

$$\frac{K_\ell^{(j)}}{dzm\ell_\ell}[\mathcal{Y}_\ell^{(j)} - \mathcal{Y}_{\ell-1}^{(j)}] + \frac{1}{2}w_\ell^{(j)}\mathcal{Y}_\ell + \frac{1}{2}w_{\ell-1}^{(j)}\mathcal{Y}_{\ell-1} = f^{(j)}; \qquad j = 1,2,3 . \tag{23}$$

This finite difference system (21)–(23) for each species can be cast as a tridiagonal system of equations

$$a_k^{(j)}\mathcal{Y}_{k-1}^{(j)} + b_k^{(j)}\mathcal{Y}_k^{(j)} + c_k^{(j)}\mathcal{Y}_{k+1}^{(j)} = fc_k^{(j)} \qquad 0 \le k \le \ell \quad j = 1,2,3 , \tag{24}$$

with

$$a_0^{(j)} = c_\ell^{(j)} = 0 ; \qquad j = 1,2,3 , \tag{25a}$$

and

$$c_0^{(j)} = \frac{K_0^{(j)}}{dzm\ell_z} - \frac{1}{2}w_0^{(j)} , \tag{25b}$$

$$b_0^{(j)} = -\frac{K_1^{(j)}}{dzm\ell_1} - \frac{1}{2}w_0^{(j)} ; \qquad j = 1,2,3 , \tag{25c}$$

$$a_k^{(j)} = \frac{2\Delta t}{dzm\ell_k + dzm\ell_{k+1}} \left[-\frac{K_k^{(j)}}{dzm\ell_k} + w_{k-1}^{(j)} \right] \tag{26a}$$

$$c_k^{(j)} = \frac{2\Delta t}{dzm\ell_k + dzm\ell_{k+1}} \left[-\frac{K_{k+1}^{(j)}}{dzm\ell_{k+1}} - w_{k+1}^{(j)} \right] ; \qquad j = 1,2,3 , \tag{26b}$$

$$b_k^{(j)} = 1 - (a_k^{(j)} + c_k^{(j)}) - \Delta t m_{jj} \qquad j = 1,2,3 \qquad 1 \le k \le \ell - 1 , \tag{26c}$$

$$b_\ell^{(j)} = +\frac{K_\ell^{(j)}}{dzm\ell_\ell} + \frac{1}{2}w_\ell^{(j)} , \tag{27a}$$

$$a_\ell^{(j)} = -\frac{K_\ell^{(j)}}{dzm\ell_\ell} + \frac{1}{2}w_{\ell-1}^{(j)} ; \qquad j = 1,2,3. \tag{27b}$$

The system of equations (24) is solved iteratively as follows: Set $e_0^{(j)} = d_0^{(j)} = 0$, and

$$e_k^{(j)} = -\frac{c_k^{(j)}}{e_{k-1}^{(j)}a_k^{(j)} + b_k^{(j)}} \tag{28}$$

$$d_k^{(j)} = \frac{fc_k^{(j)} - d_{k-1}^{(j)}a_k^{(j)}}{e_{k-1}^{(j)}a_k^{(j)} + b_k^{(j)}} ; \qquad k = 1,\ldots,\ell . \tag{29}$$

Once $e_k^{(j)}$, $d_k^{(j)}$ have been determined set $y_{\ell+1}^{(j)} = 0$, and proceeding backwards on the index k set

$$y_k^{(j)} = e_k^{(j)}y_{k+1}^{(j)} + d_k^{(j)} \qquad k = \ell,\ldots,1 , \tag{30}$$

(c) Integral Properties

After multiplying (21) by

$$s_k = \frac{1}{2} \left(dzm\ell_k + dzm\ell_{k+1} \right)$$

and adding from $k = 1$ to $\ell - 1$ we obtain after assuming $w_k^{(j)} = w_{k+1}^{(j)}$; $k = 0, \ldots, \ell - 1$:

$$\bar{N}^{\mathcal{J}+1} = \bar{N}^{\mathcal{J}} + \Delta t \sum_{j=1}^{3} (f^{(j)})^{\mathcal{J}+1}; \qquad \mathcal{J} = 1, 2, \ldots , \tag{31}$$

where

$$\bar{N}^{\mathcal{J}} = \sum_{j=1}^{3} (\bar{N}^{(j)})^{\mathcal{J}}$$

and

$$(\bar{N}^{(j)})^{\mathcal{J}} = \frac{1}{2} dzm\ell_1 \, n_0^{(j)\mathcal{J}} + \sum_{k=1}^{\ell-1} s_k n_k^{(j)\mathcal{J}} + \frac{1}{2} dzm\ell_\ell n_\ell^{(j)\mathcal{J}}.$$

Equation (31) is the discrete version of the total nitrogen content equation (11)

(d) Convergence and Positivity of Discrete Solutions

The iterations (28)–(30) are stable if

$$b_k^{(j)} \geq 1 + |a_k^{(j)} + b_k^{(j)}|; \qquad j = 1, 2, 3 , \tag{32}$$

and the nonlinear iterations (15) converge for sufficiently small Δt since if $y_p = C_p(\Delta t) y_{p-1}$ and $\|C\| \leq 1$ for Δt small.

The numerical calibration consists in the selection of the parameters $\epsilon^{(j)}$, grid spacing $dzm\ell_k$, and Δt such that the nonlinear iteration converges with a reasonable number of iterations, and the conservation law (31) holds within roundoff accuracy.

14

I now consider conditions for which the scheme (28)–(30) maps positive functions onto positive functions. First it is convenient to explore the case $w^{(1)} = w^{(3)} = 0$, $w^{(2)} = -w_{\text{sink}}$; since for our application w_{sink} can be two orders of magnitude larger than the fluid advection velocities.

$n^{(2)}$ Boundary Condition

Free Surface. The discrete boundary condition at the free surface

$$-K_1^{(2)} \frac{n_0^{(2)} - n_1^{(2)}}{dzml_1} + \frac{1}{2} w_0^{(2)} n_0^{(2)} + \frac{1}{2} w_1^{(2)} n_1^{(2)} = 0 ;$$

where I have used $w_j^{(2)} = -w_{\text{sink}}$, are simplified to the form

$$n_0^{(2)}(1 + \alpha_1^{(2)}) + n_1^{(2)}(1 - \alpha_1^{(2)}) = 0 ;$$

with

$$\alpha_i^{(2)} = 2K_i^{(2)}/(w_{\text{sink}} \, dzml_i).$$

We ensure that $n^{(2)}$ is nonnegative at the boundary provided

$$\alpha_i^{(2)} > 1 ; \qquad i = 1 . \tag{33}$$

A sufficient condition for (33) is to set the maximum step size:

$$dzml_i < K_i^{(2)}/w_{\text{sink}} . \tag{34}$$

Within the mixing layer $K^{(i)}$ increases by two orders of magnitude and (34) is easy to satisfy; whereas below the mixing layer a condition similar to (34) requires rather small grid sizes.

Bottom Boundary. At the bottom

$$-\Delta t f^{(2)} = -K_\ell^{(2)} \frac{n_{\ell-1}^{(2)} - n_\ell^{(2)}}{dzm\ell_\ell} + \frac{1}{2} w_\ell^{(2)} n_\ell^{(2)} + \frac{1}{2} w_{\ell-1}^{(2)} n_{\ell-1}^{(2)}$$

simplifies to

$$n_\ell^{(2)}(1 - \alpha_\ell^{(2)}) + n_{\ell-1}^{(2)}(1 + \alpha_\ell^{(2)}) = +\frac{2\Delta t f^{(2)}}{w_{\text{sink}}} .$$

For sufficiently small Δt, condition (34) with $i = \ell$ suffices in order to ensure nonnegative $n^{(2)}$ values, and for positive flux $f^{(2)} > 0$ the 'adaptive' condition

$$(1 + \alpha_\ell^{(2)})n_{\ell-1}^{(2)} \geq 2\Delta t f^{(2)}/w_{\text{sink}} ,$$

is necessary in order to ensure non negative $n_\ell^{(2)}$ values. No such condition is necessary if the flux is negative at the boundary. [†]

Sufficient conditions for $n^{\mathcal{J}} \geq 0$.

From (30) we can see that $n^{\mathcal{J}-1} \geq 0$, $d \geq 0$, $e \geq 0$ implies $n^{\mathcal{J}} \geq 0$.

I will now find sufficient conditions for the inequalities $e \geq 0$, $d \geq 0$.

a) $e \geq 0$. If $0 \leq e_{k-1}^{(j)} \leq 1$, $a_k^{(j)} \leq 0$, $c_k^{(j)} \leq 0$, then $e_{k-1}^{(j)} a_k^{(j)} + b_k^{(j)} = 1 - c_k^{(j)} - a_k^{(j)}(1 - e_{k-1}^{(j)}) - \Delta t\, m_{jj} \geq 1 - c_k^{(j)} - \Delta t\, m_{jj}$. It suffices then $\Delta t\, m_{jj} < 1$ to ensure $0 \leq e_k^{(j)} \leq 1$. For $j = 2, 3$ $m_{jj} \leq 0$; thus $e \geq 0$ if:

$$a_k^{(j)} \leq 0, \qquad b_k^{(j)} \leq 0, \qquad \Delta t\, M_{11} < 1 . \tag{35}$$

[†] In our application we will often use the condition

$$f^{(3)}(t) = f^{(3)}(0) \geq 0 ; \qquad t \geq 0$$

$$f^{(2)}(t) + f^{(3)}(t) = 0 ; \qquad t \geq 0.$$

In this instance the adaptive time stepping condition will not be necessary.

b) $d \geq 0$. Assuming (35) and $d_{k-1}^{(j)} > 0$, $fc_k^{(j)} - d_{k-1}^{(j)} a_j^{(j)} \geq 0$ is trivially satisfied for $j = 1, 2$; whereas for $j = 3$ it suffices

$$\Delta t \left(\frac{(\lambda f_p / t_{\max}) n_k^{(1)}}{n_k^{(3)} + \bar{n}_k^{(3)}} - k_D \right) < 1 \, . \tag{36}$$

Comment Notice that the condition (35) for the coefficients $a_k^{(j)}$, $c_k^{(j)}$ depend upon the mesh size condition

$$dzml_k < \min_j \left(\frac{K_k^{(j)}}{|w_k^{(j)}|}, \frac{K_{k+1}^{(j)}}{|w_{k+1}^{(j)}|} \right) \, , \tag{37}$$

whereas the uptake process limits the time step size. For typical values of diffusivity and vertical velocities $K/w \sim 10$ meters whereas for typical sinking speeds $K/w_{\mathrm{sink}} \sim \frac{1}{2}$ meter. It is for this reason that we investigate an alternate scheme to overcome the excessive grid refinement implied by (37).

4.2 Second Algorithm.

To overcome, to some extent, the computational constraints of the fast sinking process, I introduce time splitting algorithms. Setting

$$\mathbf{C} = \mathbf{W}_s \partial_z \mathbf{n} \tag{38a}$$

$$\mathbf{A} = \mathbf{W}_a \partial_z \mathbf{n} - \mathbf{M} \mathbf{n} - \partial_z (\mathbf{K} \partial_z \mathbf{n}) \, , \tag{38b}$$

where

$$W = \mathbf{W}_a + \mathbf{W}_s; \qquad \mathbf{W}_a = \begin{bmatrix} w & 0 & 0 \\ 0 & w & 0 \\ 0 & 0 & w \end{bmatrix} ; \qquad \mathbf{W}_s = \begin{bmatrix} 0 & 0 & 0 \\ 0 & w_{\mathrm{sink}} & 0 \\ 0 & 0 & 0 \end{bmatrix} \, . \tag{38c}$$

17

we write (2) in the form

$$\partial_t \mathrm{n} + C\mathrm{n} + A\mathrm{n} = 0 \ .$$

I will consider two algorithms. The first and simplest algorithm has $O(\Delta t)$ convergence; whereas the second one is slightly more complicated, but has $O(\Delta t^2)$ convergence.

(a) Time Implicit

$$\frac{\mathrm{n}^{\mathcal{J}+1/2} - \mathrm{n}^{\mathcal{J}}}{\Delta t} + C^{\mathcal{J}+1}\mathrm{n}^{\mathcal{J}+1/2} = 0 \ ,$$

$$\frac{\mathrm{n}^{\mathcal{J}+1} - \mathrm{n}^{\mathcal{J}+1}}{\Delta t} + A^{\mathcal{J}+1}\mathrm{n}^{\mathcal{J}+1/2} = 0 \ .$$

or, in more detail

$$\frac{\tilde{\mathrm{n}}^{\mathcal{J}+1} - \mathrm{n}^{\mathcal{J}}}{\Delta t} + W_s \partial_z \hat{\mathrm{n}}^{\mathcal{J}+1} = 0 \ , \tag{39a}$$

$$\frac{\mathrm{n}^{\mathcal{J}+1} - \tilde{\mathrm{n}}^{\mathcal{J}}}{\Delta t} - M[\mathrm{n}^{\mathcal{J}+1}]\mathrm{n}^{\mathcal{J}+1} - \partial_z [K^{\mathcal{J}+1}\partial_z \mathrm{n}^{\mathcal{J}+1}] + W_a \partial_z \mathrm{n}^{\mathcal{J}+1} = 0 \ , \tag{39b}$$

$$\mathrm{n}^0 = \hat{\mathrm{n}} \ , \tag{39c}$$

The boundary conditions are

$$\left(\tilde{n}^{(2)} \right)^{\mathcal{J}+1} = 0 \quad \text{at} \quad z = 0 \ , \tag{30e}$$

and (5) after replacing W by W_a.

In fact (39b) is (14a) after we replace W by W_a and the first algorithm in 4.1 can be used in its solution. In (39b) the term w_{sink} is missing. In this section, I concentrate on

18

the sinking process (39a). Since the process pertains only to big particulates we simplify (39a) to the form $\tilde{n}^{(1)} = n^{(1)}$, $\tilde{n}^{(3)} = n^{(3)}$, and

$$\frac{\tilde{n}^{(2)} - n^{(2)}}{\Delta t} - w_{\text{sink}} \frac{\partial n^{(2)}}{\partial z} = 0 \ . \tag{39a'}$$

I approximate (39a') using the upstream difference scheme

$$\tilde{n}_0^{(2)} = 0 \qquad \tilde{n}_k^{(2)} - \frac{\Delta t w_{\text{sink}}}{dzm\ell_k} \left(\tilde{n}_{k-1}^{(2)} - \tilde{n}_k^{(2)} \right) = n_k^{(2)} \ ; \qquad k = 0, \ldots, \ell - 1 \ . \tag{40}$$

The solution of (40) is given by·

$$a_k = \frac{\Delta t w_{\text{sink}}}{dzm\ell_k} \ ; \qquad k = 0, \ldots, \ell \ , \tag{41a}$$

$$\tilde{n}_0^{(2)} \ ; \qquad \tilde{n}_k^{(2)}(1 + a_k) = \tilde{n}_{k-1}^{(2)} a_k + n_k^{(2)} \ ; \qquad k = 1, \ldots, \ell \tag{41b}$$

The scheme (40) has the property $n^{(2)} \geq 0$ then $\tilde{n}^{(2)} \geq 0$; since $a_k > 0$, $n_k^{(2)} \geq 0$ implies $\tilde{n}_k^{(2)} \geq 0$; furthermore, (40) is unconditionally stable.

5. Diagnosis

(a) Preliminaries.

The ecological system governed by (2) lies in the upper ocean ($\sim$200 m). The uptake

$$u(z,t) = \lambda \frac{f_p n^{(3)} n^{(1)} / l_{\max}}{n^{(3)} + \bar{n}^{(3)}} , \qquad (12)$$

is light limited and nutrient limited. Only the upper layers ($<$ 100 m) have sufficient light during the day, and nutrients are essentially supplied from the lower layers. The vertical diffusivity has a strong discontinuity at the bottom of the mixing layer, and as a consequence time and space scales can not be readily defined globally. The characterization of the behavior of system (2) via non dimensional parameters is therefore complex. It is advantageous to explore this ecological system in reduced subsets of the parameter space; in particular we select some groupings of parameters to represent *seasonal* regimes.

In this section, I introduce some non-dimensional parameters useful in exploring seasonal responses.

The instantaneous euphotic depth h_e is defined by the condition

$$\lambda(-h_e, t) = \lambda_0 , \qquad (13)$$

where usually $\log_{10}(\lambda(0,t)/\lambda_0) \approx 2$. The seasonal average $\bar{h}_e$ is the time average of $h_e(t)$ (over a period of 4 months). For the mixing layer depth $h_m(t)$ I likewise introduce a seasonal average $\bar{h}_m$. It is to be noticed that the daily variability might be substantial (e.g., $\langle |h_m(t) - \bar{h}_m| \rangle_a \sim \bar{h}_m$ in Spring); and due care in the use of average scalings is required.

20

The average euphotic depth is sensitive to water mass changes and latitude (length of day); whereas the averaged mixing layer depth depends upon the season and requires in addition to the mean a prescription of a seasonal trend, $\overline{h'_m} = \overline{\frac{dh_m}{dt}}$ e.g., deepening in the Fall, steady in the Winter, etc.

The seasonal regime can be characterized therefore by a triplet $\bar{h}_e$, $\bar{h}_m$, and $\overline{h'_m}$. The time scale in the mixing layer is

$$t_m = \frac{\bar{h}_e^2}{K_m} , \qquad (44)$$

and below the mixing layer, the time scale is

$$t_b = \frac{\bar{h}_e^2}{K_b} . \qquad (45)$$

The former $\sim 10^4/10^5$ days is too short, whereas the latter $\sim 10^4/10$ days has a several year time scale; thus the fraction of the euphotic zone

$$\eta_m = 1 - \frac{\bar{h}_m + \bar{h}'_m T/2}{\bar{h}_e} , \qquad (46)$$

exposed to slow diffusivity characterizes the effect of mixing in the ecosystem. Here T is the seasonal time scale. Since the sinking of large particles and diffusivity in the mixing layer are fast processes; we seek relevant seasonal trends in time scales given by t_b and the advection scale

$$t_a = \bar{h}_e/w , \qquad (47)$$

$(\sim 10^2/1$ days).

Below the euphotic zone uptake essentially ceases and system (2) decouples somewhat. There, the dissolved nitrogen (DIN) receives small particulates with a time scale $t_m = 1/k_D$, and the particulates have relaxation time

$$t_{\text{part}} = \frac{1}{k_{12} + k_{21}} . \qquad (48)$$

21

Both t_m and t_{part} are small compared to t_b.

At a given depth h, the instantaneous residence time $t_h^{(j)}$ is defined implicitly

$$\int_{-h}^{0} n^{(j)}(z,t)dz = t_j^{(j)} \left[K \frac{\partial n^{(j)}}{\partial z} + w^{(j)} n^{(j)} \right]\Big|_{z=-h} ,$$

or in terms of the average

$$\langle n^{(j)} \rangle_h = \frac{1}{h} \int_{-h}^{0} n^{(j)}(z,t)dz , \tag{49}$$

$$h \langle n^{(j)} \rangle_h = t_j^{(j)} \left[K \frac{\partial n^{(j)}}{\partial z} + w^{(j)} n^{(j)} \right]\Big|_{z=-h} . \tag{50}$$

Assuming $K \frac{\partial n^{(j)}}{\partial z} \sim K \frac{\langle n^{(j)} \rangle_h}{\eta_m h_e}$, the time scale for the residence time in the layer above $z = -h$ is given by $t_h^{(j)}$; where

$$\left(\frac{h}{\bar{h}_e} \right) \frac{1}{t_h^{(j)}} = \frac{1}{\eta_m t_b} + \frac{1}{t_a^{(j)}} . \tag{51}$$

For big particulates $(j = 2)$ $\quad t_a \simeq \frac{h}{w_{sink}} << t_b$ that in the residence time is controlled by the gravitationally driven sinking. Both small particulate and uptake depend upon diffusivity and fluid vertical advection. Deep penetration of the mixing layer η_m small shortens the residence time when the residence time is diffusion dominated. Notice that residence time is not directly dependent upon uptake details.

The dimensional analysis above suggest $\bar{h}_e$ and t_b as the natural space and time scales with derived parameters η_m,

$$r_{up} = \left[\frac{1 + \bar{n}^{(3)}/\overline{\langle n^{(3)} \rangle}_{h_e}}{\lambda(0)} \right] \frac{(t_{max}/f_b)}{t_b} , \tag{52}$$

22

$$\tau_{\text{part}} = \frac{1}{t_b(k_{12} + k_{21})} \,, \qquad (53)$$

$$\tau_{\text{adv}} = \max_j(t_a^{(j)}/t_b) \,, \qquad (54)$$

$$\tau^{(j)} = 1 \left/ \left(\frac{1}{\eta_m} + \frac{1}{\tau_{\text{adv}}} \right) \right. . \qquad (55)$$

The time scales are known *a priori* except for the uptake time scale that depends upon system response ($\langle n^{(?)} \rangle_{h_e}$).

In this parameter space the seasonality enters in the parameter η_m and possibly in the seasonality of the upwelling/downwelling $\tau_{\text{adv}} = (w\bar{h}_e/K)$.

6. Calibration and Model results

The model was initialized with data typical for the Bermuda region (Altabet, 1989). Parameter sensitivities were tested with runs of 150 to 300 days under steady conditions. Runs to test responses to seasonal variations in mixed layer depth and surface light intensity were also made. All our runs used algorithm 4.1. Time step was 0.5 hr. and vertical resolution was 0.5 m. The latter was found to be a necessary condition for stability and convergence in the equations governing BPN sinking. The algorithm 4.2 permits coarser level spacing but has not yet been implemented. Accuracy of the numerical solutions was tested by examining conservation of total nitrogen over the run (DIN + SPN + BPN for model domain) which was achieved in all cases except for the seasonal runs. In these instances, there was a 10% loss over 2 years of simulated time (Figure 3). This apparent loss was produced by roundoff errors resulting from the very high gradients in BPN within a few meters of the bottom boundary as a result of the no flux condition. The sensitivity runs were very robust with respect to the vertical distribution of properties (Figure 2 as an example). A strong nitracline was found between 80 and 120 m. In the upper 80 m, DIN concentrations were less than 0.05 mol/l and are of the order observed in the field by chemiluminescent techniques. SPN exhibits a maximum in the vicinity of the nitracline and drops off sharply below. BPN has a similar distribution but its maximum is 20 m deeper. Vertical particle flux is simply the product of BPN concentration and sinking speed (100 m/day for these runs) and during the steady state portions of the runs must equal vertical DIN flux for the 1-D case. These general features and overall magnitude of quantities are similar to observations (Altabet, 1989). Vertical fluxes are higher than measured at Bermuda in part due to a steeper vertical gradient in DIN realized by the model and can be adjusted with different initial concentrations. When the mixed layer depth (mld) is relatively shallow (40 m in these cases) the vertical positioning of the features was only sensitive to the surface light intensity I_0, the half-saturation constant for the dependence of phytoplankton growth on light ($\hat{I}_z$), and the extinction coefficient (z_0). As expected, SPN

24

and BPN concentration are sensitive to the first-order constants for their interconversion and sinking speed k_{12} and k_{21}. At low values for sinking speed w_{sink} the ratio of SPN:BPN is set by the ratio of these constants. Increased mixing in the nitracline produces higher concentrations of particles and their fluxes.

Seasonal variations in mixed layer depth and surface irradiance of similar phase and magnitude (modeled for the present as a sinusoidal variation) to those of the Bermuda region produce large changes in concentrations and vertical structure (Figure 4). Increasing the mixed layer depth to 190 m erases the subsurface features and result in surface maxima for SPN. Overall levels of SPN are higher due to increased uptake of DIN due to its increased supply to the euphotic zone by mixing. DIN concentrations are correspondingly reduced. BPN is uniform throughout the region and the vertical flux of particles at 100 m have increased by a factor of 4. Upon stratification, concentrations return to their summertime values. DIN 'grows' in below the euphotic zone due to the decay of particles. The subsurface maxima intensifies and deepens throughout the summertime period. The reproduction of the temporal pattern for the 2nd year shows that there are no long-term adjustments occurring in the model. These features of the seasonal cycle have been observed at Bermuda except for the simulated wintertime SPN and BPN which are too high (factor of 2) values for DIN which are too low (factor of 5 in euphotic zone). This in part due to the no-flux condition at the bottom. In the real world, particle flux at 200 m would draw down total N during the wintertime deep mixing conditions and thus the amount of nitrogen available to support high particulate concentrations and uptake.

7. Conclusions

This preparatory work for a full three dimensional biogeochemical model imbedded in a 3-D physical model shows that a three compartment nitrogen cycle model is capable of simulating observed nitrogen distribution in the upper ocean.

The approach to our next stage in model development are:

1) Improved light dependency parametrizations Before attachment to HOOM, the present BGC model will be expanded to include a dependence on light from particle concentrations. Feedback from this dependency in combination with BPN flux through the lower boundary should result in wintertime simulations closer to reality. Algorithms to simulate chlorophyll distributions will be developed that take into account photoadaptation.

2) Attachment to HOOM. Initially, idealized eddies and jets will be simulated and their interaction with the BGC model analyzed. The contributions and sensitivities of specific processes will be tested by selectively turning them off and on. The fidelity of HOOM in simulating isopycnal fluxes will also be analyzed at this point.

3) Further 1-D model complexity. In parallel with item 2, more complex versions of the BGC model will be developed and tested in 1-D mode. Goals for this phase of the modeling effort are the simulation of the proportion of phytoplankton nitrogen to SPN (now parameterized), recycled nitrogen fluxes, and primary production (in addition to new production). Effort will focus on adding compartments for zooplankton, bacteria, detritus, and DOM.
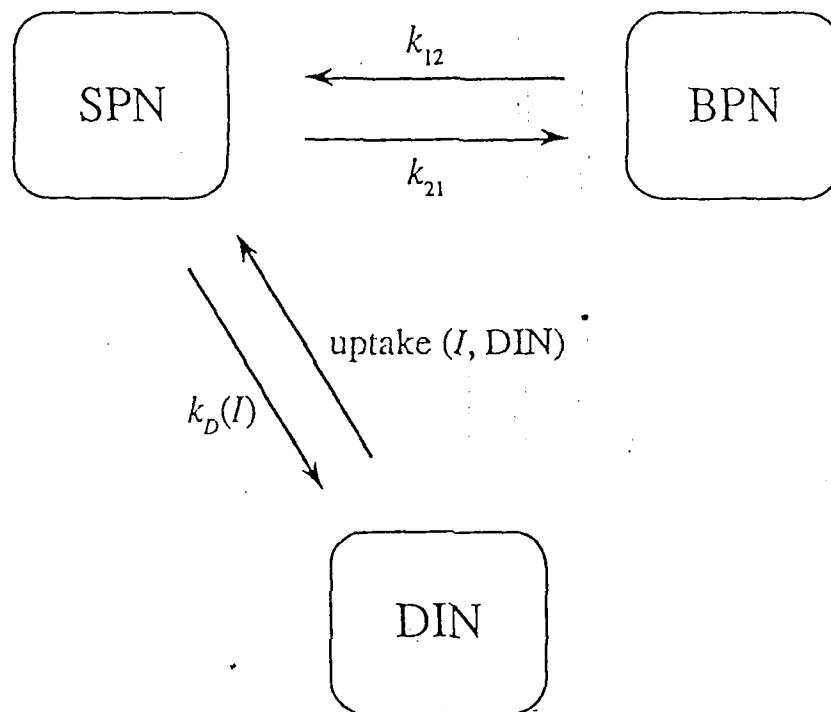
a) Local nitrogen exchanges
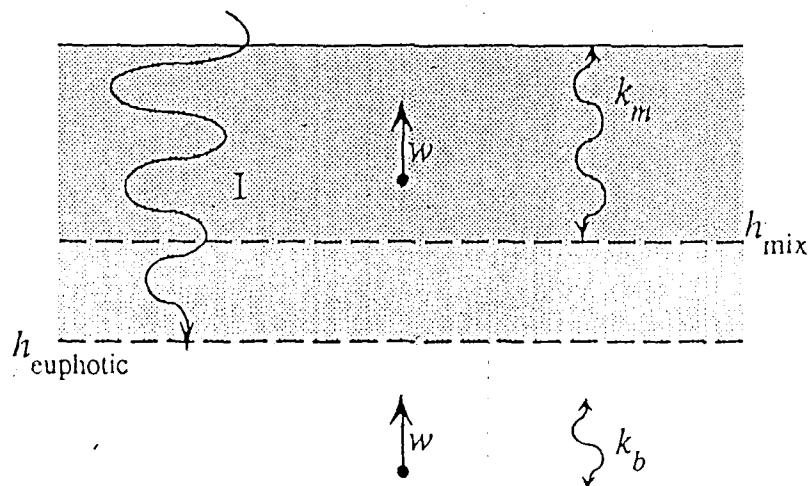
b) Physical fields influencing
   nitrogen vertical distribution

Figure 1. A 1-dimensional Upper Ocean Biogeochemical Model
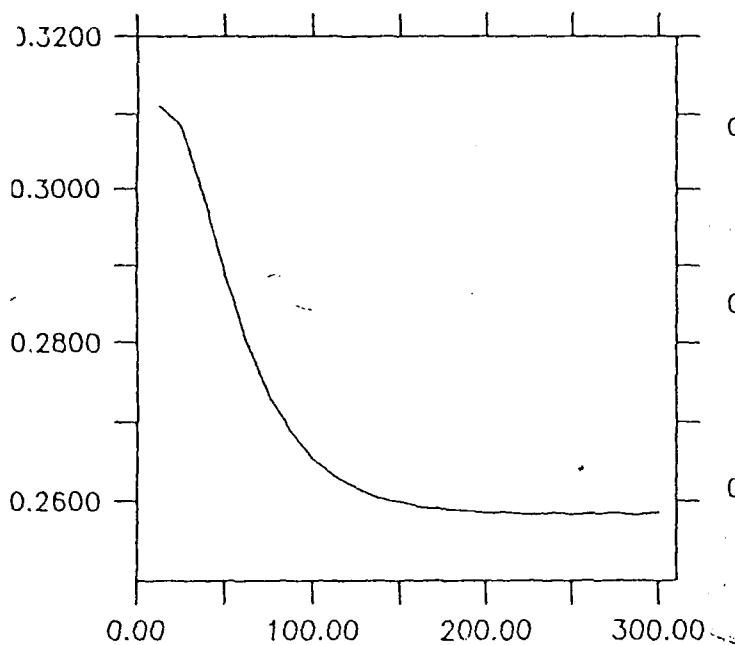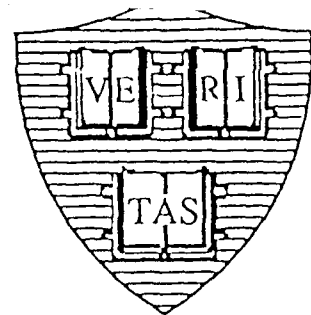
(a) Small Particulate

sensitivity_1"
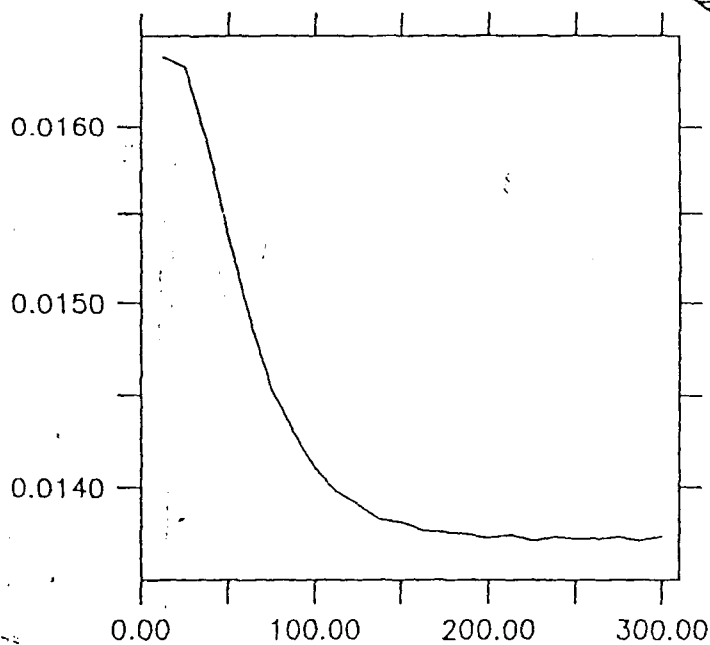
(b) Big Particulate
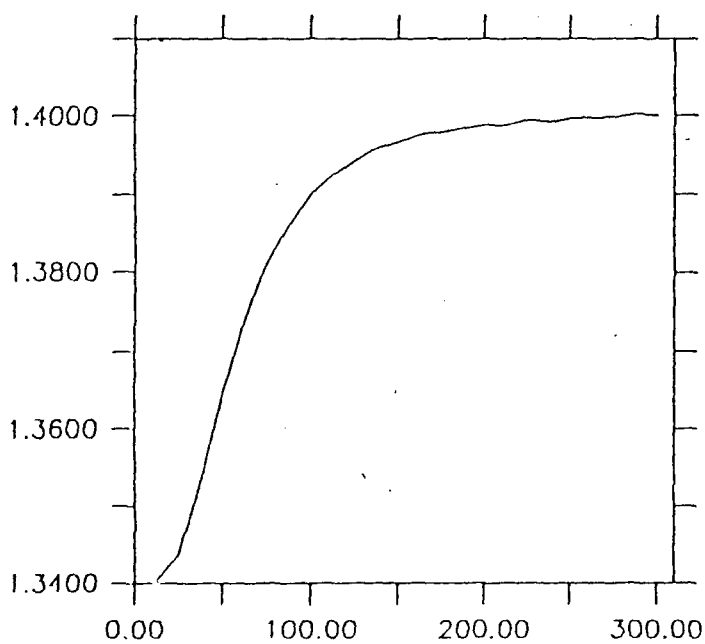
(c) Dissolved Nitrogen
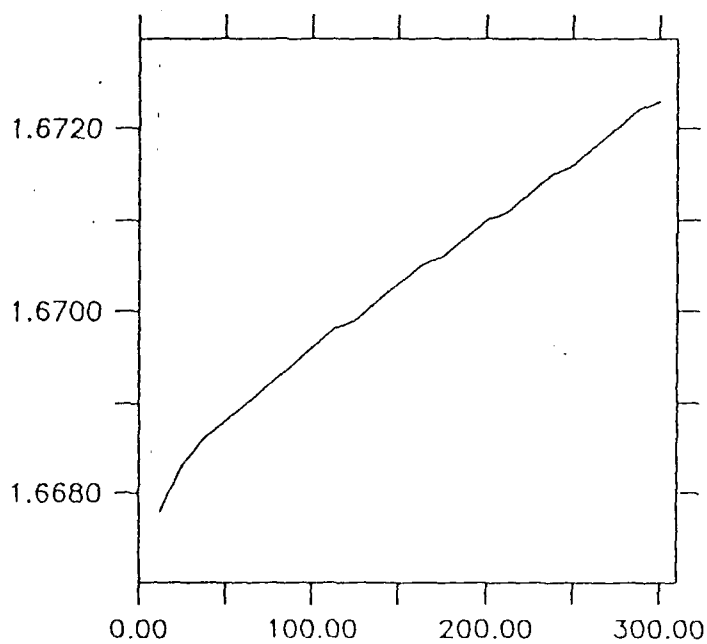
(d) Total Nitrogen Content

Figure 2. Example of a sensitivity run time history of
vertically integrated nitrogen on each compartment and
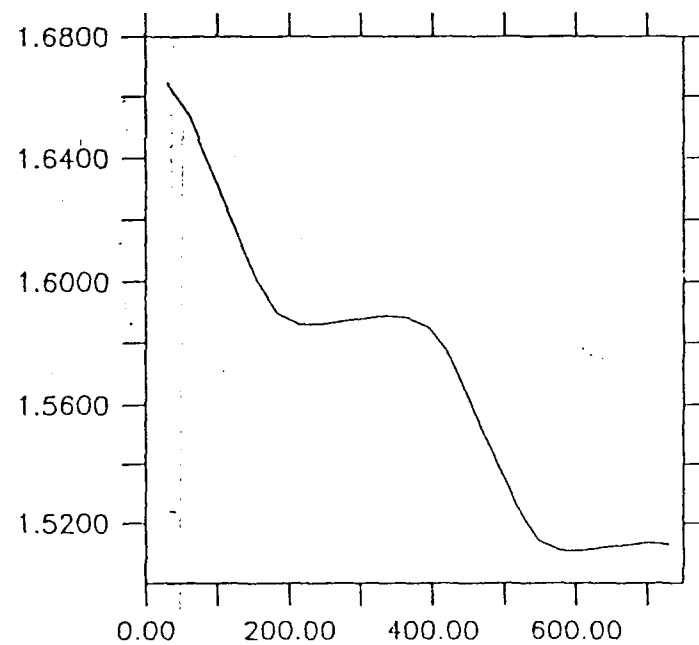total one year scale.
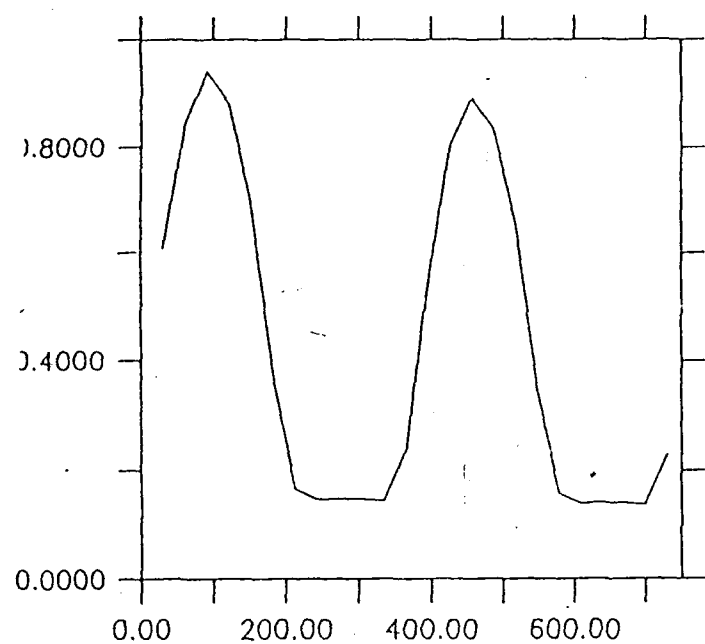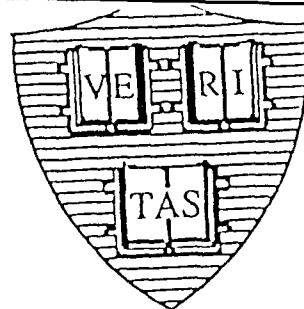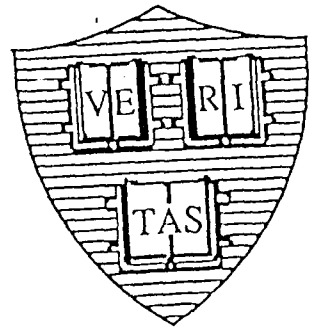
(a) Small Particulate
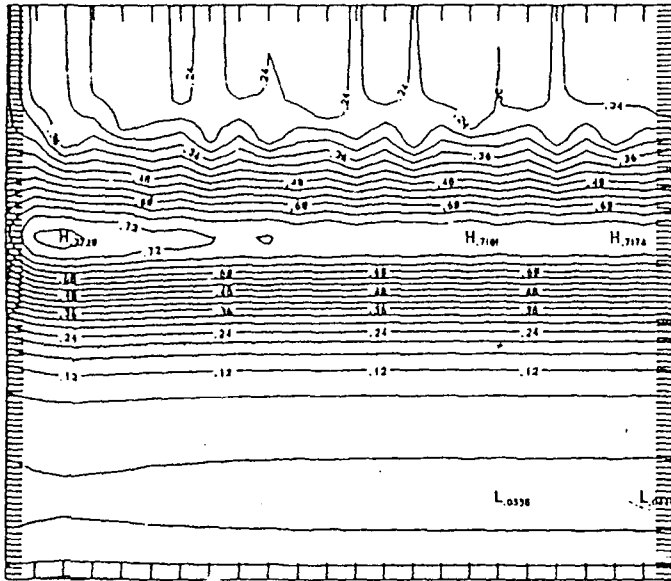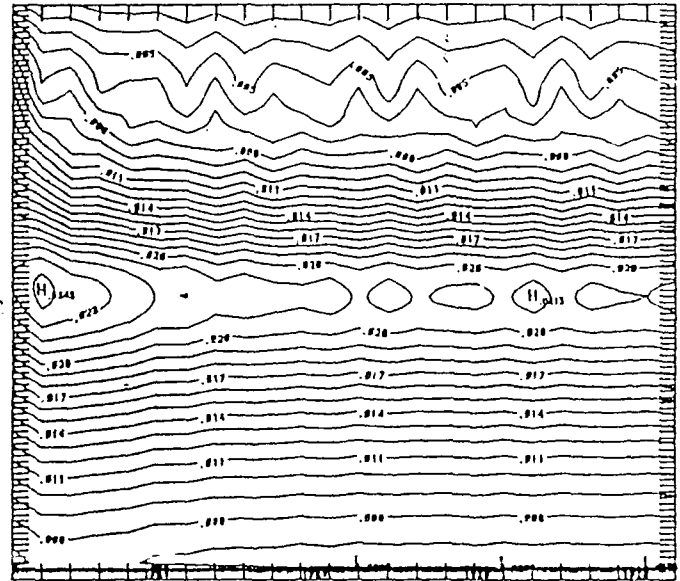
seasonal_6"
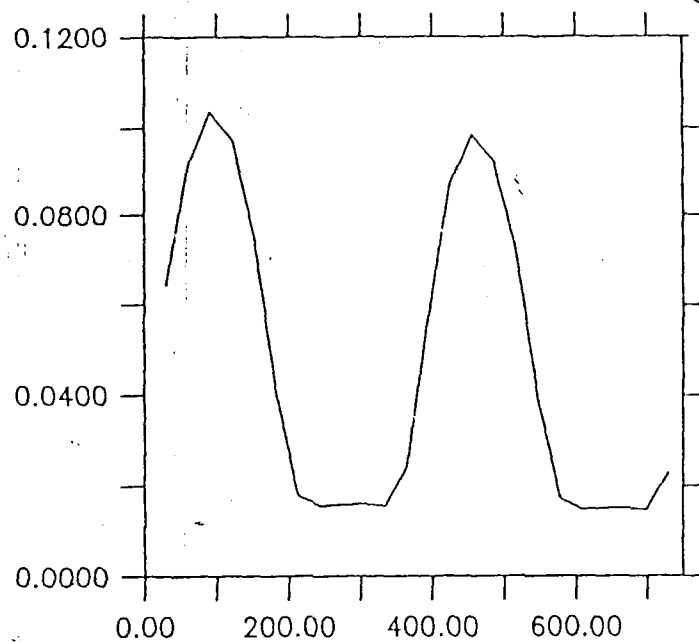
(b) Big Particulate
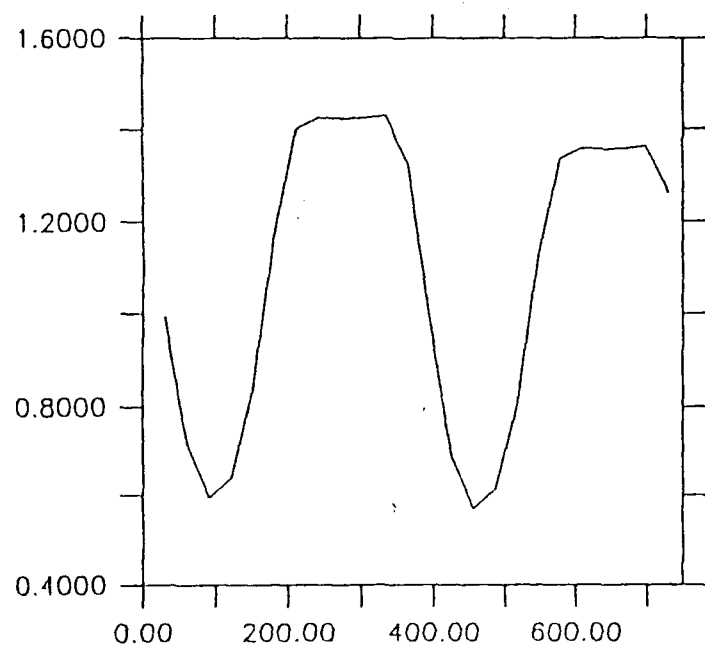
(c) Dissolved Nitrogen

(d) Total Nitrogen Content

Figure 3. Same as Figure 2, but for a long term run.

Figure 4. Example of sensitivity run depth versus time
contours of nitrogen compartments and totals.
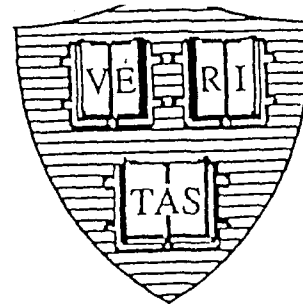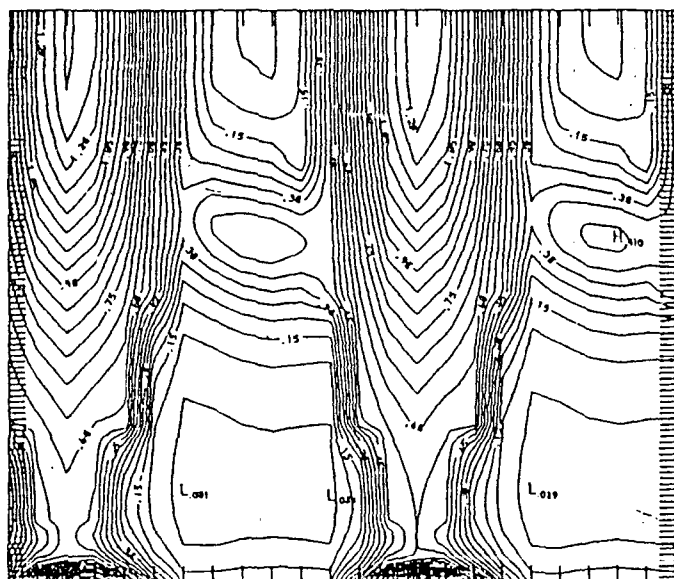
CONTOUR FROM .05 TO 1.3 BY .05 (X 1)
Small Particulate Nitrogen (mmol/m 3) at time   0.0
[0.0295, Mean: 0.4320 , 1.3128]
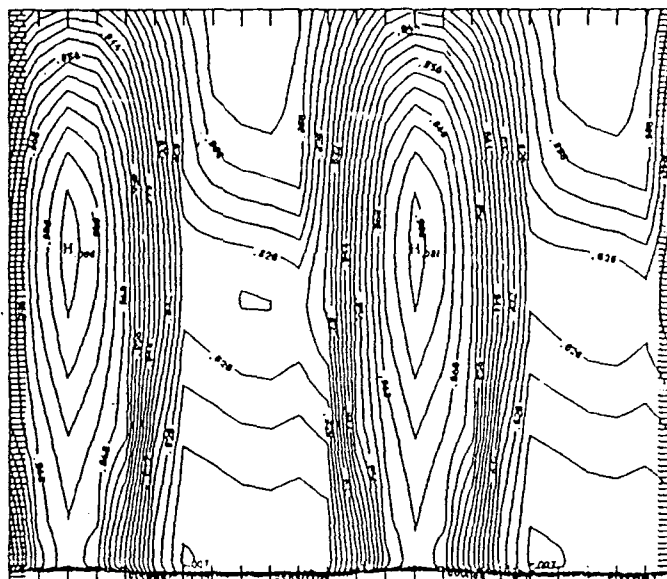
CONTOUR FROM 0 TO .1 BY .004 (X 1)
Big Particulate Nitrogen (mmol/m 3) at time   0.0
[0.0006, Mean: 0.0738 , 9.3946]

0 m

600 m
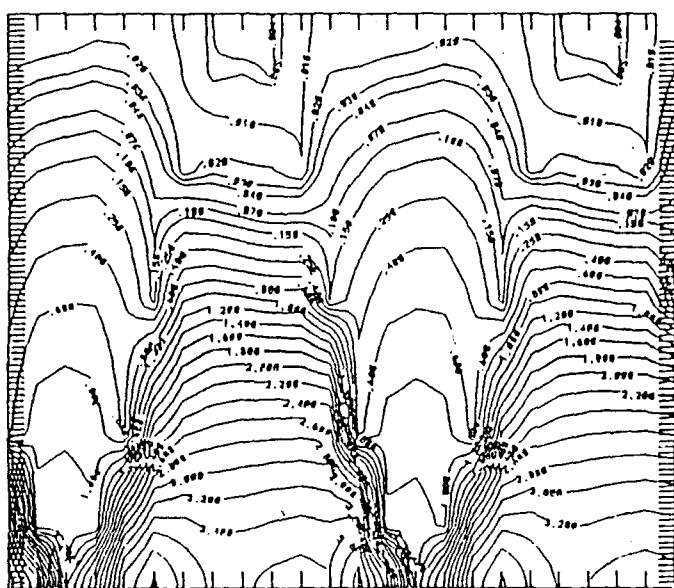
CONTOUR FROM 0 TO 4 BY 0 (X 1)
Dissolved Nitrogen (mmol/m 3) at time   0.0
[0.0031, Mean: 1.0975 , 4.1014]
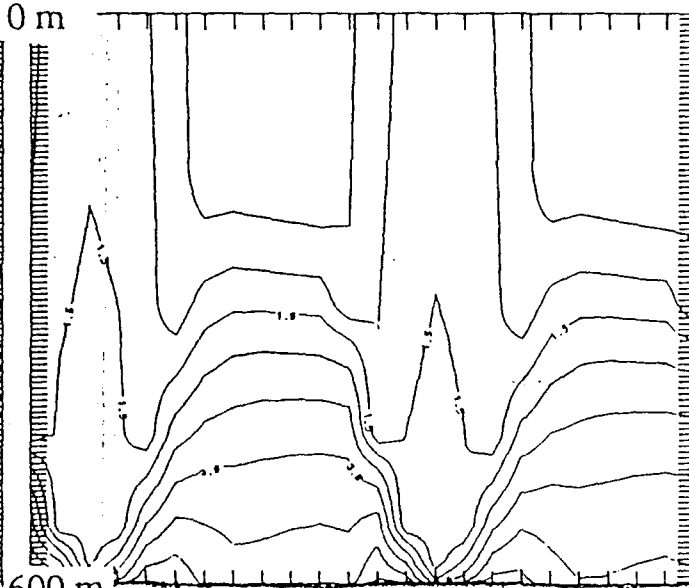
CONTOUR FROM .5 TO 12.5 BY .5 (X 1)
Total Nitrogen (mmol/m 3) at time   0.0
[0.0433, Mean: 1.6033 ,12.5510]

Figure 5. Same as Figure 4 but for a long term run.